

Evolution of electrical and magnetotransport properties with lattice strain in $La_{0.7}Sr_{0.3}MnO_3$ film

Zhi-Bin Ling(令志斌), Qing-Ye Zhang(张庆业), Cheng-Peng Yang(杨成鹏), Xiao-Tian Li(李晓天), Wen-Shuang Liang(梁文双), Yi-Qian Wang(王乙潜), Huai-Wen Yang(杨怀文), Ji-Rong Sun(孙继荣)

Citation: Chin. Phys. B . 2020, 29(9): 096802 . **doi:** 10.1088/1674-1056/aba09b
Journal homepage: http://cpb.iphy.ac.cn; http://iopscience.iop.org/cpb

What follows is a list of articles you may be interested in

Tuning the alignment of pentacene on copper substrate by annealing-assistant surface functionalization

Qiao-Jun Cao(曹巧君), Shuang Wen(温爽), Hai-Peng Xie(谢海鹏), Bi-Yun Shi(施碧云), Qun Wang(王群), Cong-Rong Lu(卢从蓉), Yongli Gao(高永利), Wei-Dong Dou(窦卫东)

Chin. Phys. B . 2020, 29(7): 076801 . **doi:** 10.1088/1674-1056/ab8da2

Epitaxial fabrication of two-dimensional $TiTe_2$ monolayer on Au(111) substrate with Te as buffer layer

Zhipeng Song(宋志朋), Bao Lei(雷宝), Yun Cao(曹云), Jing Qi(戚竞), Hao Peng(彭浩), Qin Wang(汪琴), Li Huang(黄立), Hongliang Lu(路红亮), Xiao Lin(林晓), Ye-Liang Wang(王业亮), Shixuan Du(杜世萱), Hong-Jun Gao(高鸿钧)

Chin. Phys. B . 2019, 28(5): 056801 . **doi:** 10.1088/1674-1056/28/5/056801

Controllable fabrication of self-organized nano-multilayers in copper-carbon films

Wei-Qi Wang(王伟奇), Li Ji(吉利), Hong-Xuan Li(李红轩), Xiao-Hong Liu(刘晓红), Hui-Di Zhou(周惠娣), Jian-Min Chen(陈建敏)

Chin. Phys. B . 2019, 28(3): 036802 . **doi:** 10.1088/1674-1056/28/3/036802

Growth and transport properties of topological insulator Bi_2Se_3 thin film on a ferromagnetic insulating substrate

Shanna Zhu(朱珊娜), Gang Shi(史刚), Peng Zhao(赵鹏), Dechao Meng(孟德超), Genhao Liang(梁根豪), Xiaofang Zhai(翟晓芳), Yalin Lu(陆亚林), Yongqing Li(李永庆), Lan Chen(陈岚), Kehui Wu(吴克辉)

Chin. Phys. B . 2018, 27(7): 076801 . **doi:** 10.1088/1674-1056/27/7/076801

Effect of hydroxyl on dye-sensitized solar cells assembled with TiO_2 nanorods

Lijian Meng(孟立建), Tao Yang(杨涛), Sining Yun(云斯宁), Can Li(李灿)

Chin. Phys. B . 2018, 27(1): 016802 . **doi:** 10.1088/1674-1056/27/1/016802

Evolution of electrical and magnetotransport properties with lattice strain in $La_{0.7}Sr_{0.3}MnO_3$ film*

Zhi-Bin Ling(令志斌)[1,†], Qing-Ye Zhang(张庆业)[1,†], Cheng-Peng Yang(杨成鹏)[1,†], Xiao-Tian Li(李晓天)[1], Wen-Shuang Liang(梁文双)[1], Yi-Qian Wang(王乙潜)[1,‡], Huai-Wen Yang(杨怀文)[2], and Ji-Rong Sun(孙继荣)[2]

[1] *College of Physics & State Key Laboratory, Qingdao University, Qingdao* 266071, *China*

[2] *Beijing National Laboratory for Condensed Matter Physics, Institute of Physics, Chinese Academy of Sciences, Beijing* 100190, *China*

(Received 9 May 2019; revised manuscript received 3 June 2020; accepted manuscript online 29 June 2020)

In this paper, we investigate the effects of lattice strain on the electrical and magnetotransport properties of $La_{0.7}Sr_{0.3}MnO_3$ (LSMO) films by changing film thickness and substrate. For electrical properties, a resistivity upturn emerges in LSMO films, *i.e.*, LSMO/STO and LSMO/LSAT with small lattice strain at a low temperature, which originates from the weak localization effect. Increasing film thickness weakens the weak localization effect, resulting in the disappearance of resistivity upturn. While in LSMO films with a large lattice strain (*i.e.*, LSMO/LAO), an unexpected semiconductor behavior is observed due to the linear defects. For magnetotransport properties, an anomalous in-plane magnetoresistance peak (pMR) occurs at low temperatures in LSMO films with small lattice strain, which is caused by two-dimensional electron gas (2DEG). Increasing film thickness suppresses the 2DEG, which weakens the pMR. Besides, it is found that the film orientation has no influence on the formation of 2DEG. While in LSMO/LAO films, the 2DEG cannot form due to the existence of linear defects. This work can provide an efficient way to regulate the film transport properties.

Keywords: LSMO film, lattice strain, electrical transport, magnetotransport

PACS: 68.37.–d, 68.37.Og, 72.15.Rn, 75.70.–i **DOI:** 10.1088/1674-1056/aba09b

1. Introduction

The hole-doped perovskite manganite $R_{1-x}A_xMnO_3$ (R: a trivalent rare-earth ion, A: a divalent alkaline-earth ion) films, a typical strongly-correlated system, has attracted extensive attention due to their fascinating physical properties.[1–6] In $R_{1-x}A_xMnO_3$, the Mn ions are in mixed valence states of Mn^{3+} and Mn^{4+}. The magnetic and transport properties of the doped manganite are associated with the motion of the itinerant e_g electrons *via* O^{2-} 2p orbitals between neighboring Mn^{3+} and Mn^{4+} based on the double exchange (DE) mechanism.[7] As is well known, the structure, magnetic, and transport properties of $R_{1-x}A_xMnO_3$ are closely related to each other due to the essential coupling of several electronic and lattice degrees of freedom. Therefore, external perturbations such as lattice strain[8] and electric field[9] can dramatically modify the physical properties of $R_{1-x}A_xMnO_3$ films.

Recently, $La_{1-x}Sr_xMnO_3$ films have become more attractive because they can be intentionally strained, resulting in a coupling between the lattice strain and the spin, orbital, charge degrees of freedom, and finally producing some unusual transport properties at low temperature.[10–14] As reported, great effort has been devoted to exploring the origins of these anomalous transport properties.[15,16] However, few studies focus on the evolution of the unexpected physical properties with lattice strain which can be adjusted by changing film thickness and substrate. A systematic understanding of the strain effect on the transport properties is still not fully established due to the complex lattice relaxation. Therefore, exploring the role of the strain effect on the transport properties is a necessary step in elucidating the evolution of the low-temperature unexpected phenomena with strain.

In this work, we investigate the effect of lattice strain on the transport properties of $La_{0.7}Sr_{0.3}MnO_3$ (LSMO) films through adjusting the film thickness and changing the substrate. A resistivity upturn is observed in the LSMO films with low lattice mismatch, which originates from the weak localization (WL) effect. The resistivity minimum is sensitive to the film mismatch magnitude and film thickness. Besides, an unexpected in-plane magnetoresistance (pMR) peak is observed, which is caused by two-dimensional electron gas (2DEG). The pMR peak is suppressed by increasing film thickness and temperature. This work can shed light on understanding the evolution of low temperature anomalous transport properties and

*Project supported by the National Natural Science Foundation of China (Grant No. 10974105), the Double-Hundred Talent Plan, Shandong Province, China (Grant No. WST2018006), the Recruitment Program of High-end Foreign Experts, China (Grant Nos. GDW20163500110 and GDW20173500154), and the Top-notch Innovative Talent Program of Qingdao City, China (Grant No. 13-CX-8). One of the authors (Yi-Qian Wang) was sponsored by the Taishan Scholar Program of Shandong Province, China, the Qingdao International Center for Semiconductor Photoelectric Nanomaterials, China, and Shandong Provincial University Key Laboratory of Optoelectrical Material Physics and Devices, China.

† These authors contributed to this work equally.

‡Corresponding author. E-mail: yqwang@qdu.edu.cn

© 2020 Chinese Physical Society and IOP Publishing Ltd

provide an efficient method to regulate the film physical properties.

2. Experiment

$La_{0.7}Sr_{0.3}MnO_3$ films respectively with a thickness of 6, 8, 10, 15, and 20 nm were epitaxially grown on $SrTiO_3$ (STO), $LaAlO_3$ (LAO) and (La, Sr)(Al, Ta)O_3 (LSAT) substrates by using a pulsed laser deposition (PLD) technique. During the deposition, the substrates were maintained at 750 °C in an oxygen pressure of 50 Pa. The laser wavelength was 248 nm, the pulse fluency was 1.5 J/cm^2, and the ablation frequency was 1 Hz. After the deposition, the films were naturally cooled down to room temperature at 50 Pa.

Specimens for transmission electron microscopy (TEM) examinations were prepared in cross-sectional orientation by using conventional techniques of mechanical polishing and ion milling. The ion milling was performed using a Gatan model 691 precision ion polishing system (PIPS). The bright-field (BF) imaging, and high-resolution TEM (HRTEM) examinations were carried out on a JEOL JEM 2100F electron microscope operated at 200 kV. The structure of each film was analyzed by x-ray diffraction (XRD) through using Riguka SmartLab x-ray diffractometer. The temperature dependent resistivity and angular-dependent magnetoresistance (MR) were measured on the physical property measurement system (PPMS, Quantum Design) equipped with a sample rotation system through using Van Der Pauw method. During the measurement, the films were rotated clockwise and the rotation axis was parallel to the sample edge. The rotational angles $\theta = 0°$ and $\theta = 90°$ refer to the magnetic field being perpendicular and parallel to the interface plane, respectively. All curves of the magnetic field-dependent magnetization (M–H) of the films were measured along the [100] direction of the substrate, with the external field applied to the film plane at 10 K.

3. Results and discussion

3.1. Structural properties

The LSMO films are epitaxially grown on STO, LSAT and LAO substrates, and the lattice mismatches are calculated to be 0.94%, −0.73%, and −2.1%, respectively. This implies that STO substrate ($a_{STO} = 3.905$ Å) exerts an in-plane tensile strain, while LSAT ($a_{LSAT} = 3.84$ Å) and LAO ($a_{LAO} = 3.792$ Å) substrates impose an in-plane compressive strain. Figure 1 shows the XRD patterns of LSMO/STO and LSMO/LAO films, where the (002) reflections are marked. For the LSMO/STO films [Fig. 1(a)], the (002) peak of film coincides with that of substrate because of similar lattice constants. For the LSMO films grown on LAO substrates [Fig. 1(b)], the (002) reflections shift toward large angles with increasing film thickness, meaning that the lattice strain is relaxed with film thickness increasing.

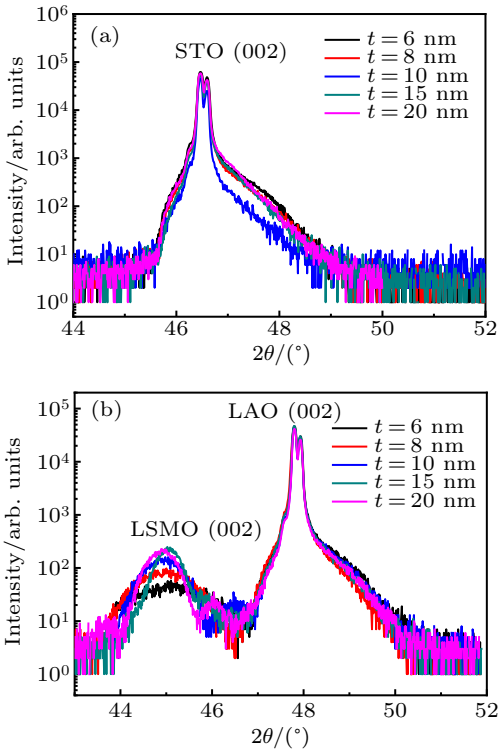


Fig. 1. XRD patterns of 6-, 8-, 10-, 15-, and 20-nm-thick LSMO film grown on STO (a) and LAO (b), respectively.

3.2. Electrical transport properties

To investigate the evolution of the film resistivity with lattice strain induced by substrate, the temperature-dependent resistivity values of LSMO films with different thickness grown on different substrates are measured. For the LSMO films grown on (001) STO substrate, which shows an in-plane tensile strain, the temperature-dependent resistivity (R *versus* T) is shown in Fig. 2(a). It is observed that the resistivity values for all samples decrease with temperature decreasing, showing a metallic behavior. Interestingly, as the temperature decreases to ∼ 25 K, the resistivity value for each of LSMO films displays a smooth upturn when the film thickness is less than 15 nm, showing a metal–insulator transition. The resistivity is fitted by using R *versus* $\ln T$ and σ *versus* $\ln T$ (*i.e.*, R^{-1} *versus* $\ln T$) curves as shown in Figs. 2(b) and 2(c). It is observed that the curves show good linear relationships when the film thickness is less than 15 nm. It is reported that the Kondo effect is manifested by the R_s upturn, which slows down and is saturated at ultra-low temperature. In contrast, owing to the WL effect, the R_s upturn will never be saturated.[17] Besides, we further investigate the resistivity minima using different models as shown in Fig. S1 in supplementary materials. It is found that the resistivity data are better fitted by the WL model. Therefore, we can reasonably deduce that the trans-

port mechanism for LSMO/LAO film is dominated by the WL according to the fitting curves of film resistivity at low temperature.

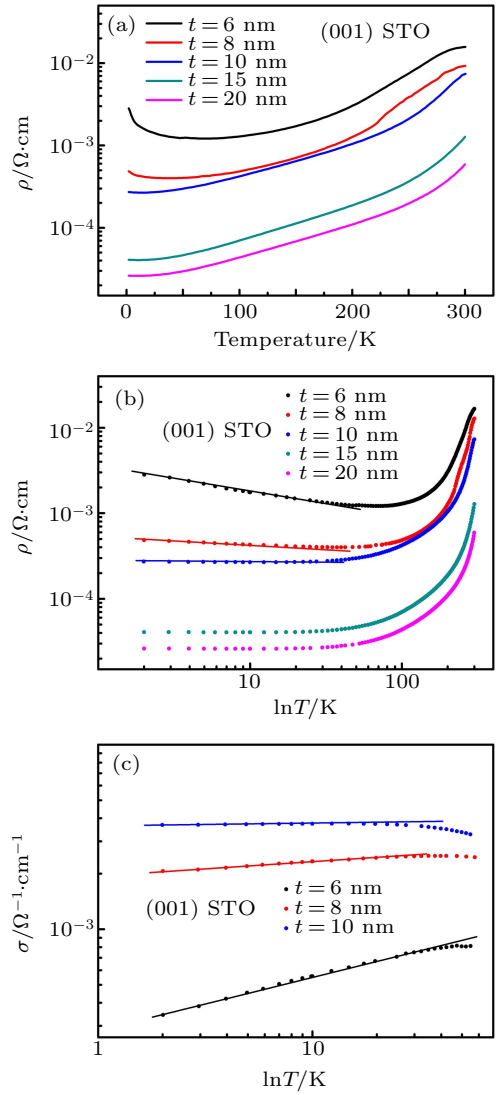


Fig. 2. (a) Temperature-dependent resistivity curves of LSMO films with different thicknesses, grown on (001) STO substrate; (b) ρ *versus* ln$T$ curves, and (c) σ *versus* ln$T$ curves derived from the data in panel (a).

To further clarify the effect of lattice strain on resistivity of the film, the R *versus* T curves of films subjected to in-plane compressive strain (*i.e.*, (001) LSAT and (001) LAO substrates) are also measured as shown in Fig. 3. It is observed that the resistivity upturn emerges only in the ultra-thin LSMO/LSAT film (Figs. S2 and S3 in supplementary materials), indicating that the WL exists only in the films subjected to small compressive strain. However, the LSMO/LAO film shows an insulator behavior below 10 nm. The film resistivity drastically decreases with film thickness increasing and shows a metallic behavior in 20-nm-thick LSMO/LAO film. The metal-insulator transition occurs at $\sim$ 260 K (Figs. S4 and S5 in supplementary materials).

As is well known, the physical properties of materials are determined by their microstructures. To clarify the different resistivity behaviors, the microstructure of the LSMO film is investigated by TEM examination in detail as shown in Fig. 4. Figure 4(a) shows a typical HRTEM image of the cross-sectional LSMO/STO sample with a thickness of 10 nm, and figure 4(b) shows its corresponding one-dimensional Fourier-filtered lattice image. The interface between film and substrate is marked by dashed lines. From Fig. 4(a), it can be clearly seen that the interface is fairly clear and sharp, and the surface is flat. The HRTEM image shows that the LSMO film grows coherently on the substrate without obvious dislocations and the interface is sharp, demonstrating a good epitaxial growth of the LSMO film. Figure 4(c) is a typical HRTEM image of a cross-sectional LSMO/LAO sample with a thickness of $\sim$ 6 nm, and figure 4(d) shows its corresponding Fourier-filtered lattice image. The interface between substrate and film is indicated by dashed lines. Some pure edge dislocations are observed from the HRTEM image, one being shown in Fig. 4(c). The extra half atomic plane can be clearly seen from the Fourier-filtered lattice image. The TEM results demonstrate that some dislocations are produced even in ultra-thin LSMO/LAO film. Therefore, the transport behavior is greatly affected by the linear defects, resulting in an insulator behavior. The lattice strain is relaxed with film thickness increasing. Therefore, the electrical transport properties of LSMO/LAO film ($t > 20$ nm) are dominated by the double exchange interaction, resulting in a metallic behavior.

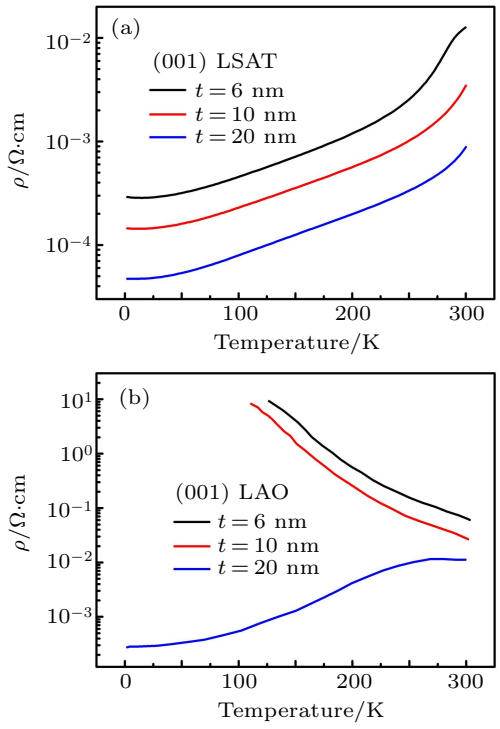


Fig. 3. Temperature-dependent resistivity curves of LSMO films grown on (a) (001) LSAT and (b) (001) LAO, respectively.

What is more, it is reported that the WL originates from the orbital effect of conduction electrons, and the electrons

can be scattered in the conduction process.[17] For the ultra-thin LSMO films grown, respectively, on STO and LSAT substrates, the lattice mismatch is very small, and the effects of linear defects can be ignored. Therefore, the double exchange interaction is responsible for the conduction in film,[19] resulting in a metallic behavior. However, the backscattering of the electron is enhanced considering the electronic interface effect at low temperature. The electrical transport behavior is dominated by the WL effect rather than the double exchange, resulting in the resistivity upturn. With temperature increasing, the electron interface effect gradually diminishes,[20] thereby weakening the WL effect and improving the conductivity. Besides, the lattice strain can be relaxed with film thickness increasing, which weakens the WL effect and enhances the double exchange, leading the conductivity to turn higher and the resistivity minimum to disappear.

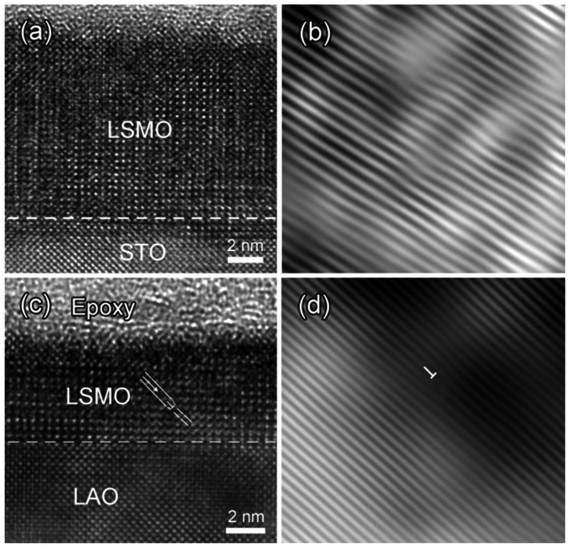


Fig. 4. (a) Typical HRTEM image and (b) corresponding one-dimensional Fourier-filtered lattice image of 10-nm-thick LSMO/STO film; (c) typical HRTEM image, and (d) corresponding one-dimensional Fourier-filtered lattice image of 6-nm-thick LSMO/LAO film.

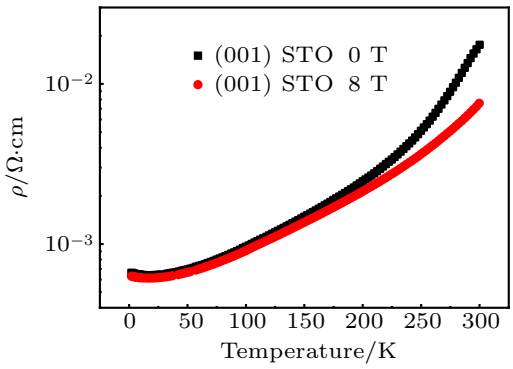


Fig. 5. Curves of temperature-dependent resistivity of 8-nm-thick LSMO films grown on (001) STO substrate under different applied magnetic fields.

To further investigate the low-temperature resistivity minima, we measure the temperature-dependent resistivity values of 8-nm-thick LSMO films grown on (001) and (011) STO substrates under different applied magnetic fields. From Figs. 5 and 6, it follows that the resistivity values of the LSMO film under 0 T and 8 T are similar to each other. However, the conductivity of LSMO film under 8 T becomes better than under 0 T with increasing temperature. Besides, it is observed that the low temperature resistivity minimum of LSMO film occurs under 8 T, which indicates that the applied magnetic field cannot affect the emergence of the WL effect. This phenomenon can also be found in 6-nm-thick LSMO film grown on STO separately under magnetic field of 0 T and 5 T as shown in Fig. S6.

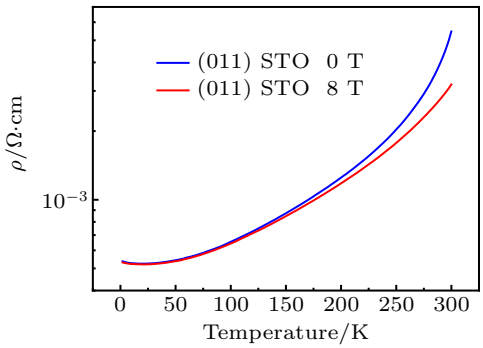


Fig. 6. Curves of temperature-dependent resistivity of 8-nm-thick LSMO films grown on (011) STO substrate under different applied magnetic fields.

3.3. Magnetotransport properties

To reveal the strain effect on the anomalous transport properties of the films, the MR properties are also investigated. Figures 7 and figure S7 show the curves of angular-dependent MR of LSMO films grown on (001) STO, (001) LSAT, and (001) LAO substrates with a thickness ranging from 6 nm to 20 nm. For the LSMO/STO films, it is observed that all samples show negative MR behaviors. Two different MR peaks are observed. When the magnetic field is perpendicular to the film surface (*i.e.*, $\theta = 0^\circ$ and 180°), an out-of-plane MR peak is observed, which is a standard resistivity maximum occurring for the ferromagnetic manganite.[21] The other one occurs when the magnetic field is parallel to the film surface (*i.e.*, $\theta = 90^\circ$ and -90°), which is called in-plane MR peak (pMR). The height of the pMR-peak decreases with film thickness increasing, and the pMR-peak disappears when the film thickness reaches 15 nm. For the LSMO films grown on (001) LSAT substrates, the evolution of angular MR with the film thickness is similar to that of LSMO/(001) STO film. For the LSMO films grown on (001) LAO substrates, negative MR behaviors are observed. However, no pMR-peak occurs when the magnetic field is parallel to the film surface (*i.e.*, $\theta = 90^\circ$ and $\theta = -90^\circ$), which is different from the angular-dependent MR behavior of LSMO/(001) STO films.

As reported, the pMR occurs due to the 2DEG caused by the interface effect in the ultra-thin LSMO film.[22] The pMR-peaks signal that the formation of a two-dimensional mangan-

ite at the film interface, decoupled from the rest of the manganite layer, which could arise from a magnetic reconstruction. The lattice strain is relaxed with film thickness increasing, which weakens the interface effect. Therefore, the 2DEG gradually disappears, decaying the pMR-peak. While for the LSMO/LAO film, the linear defects (shown in Fig. 4) exist at the film interface, which can destroy the 2DEG, resulting in the disappearance of pMR-peak as shown in Fig. S7.

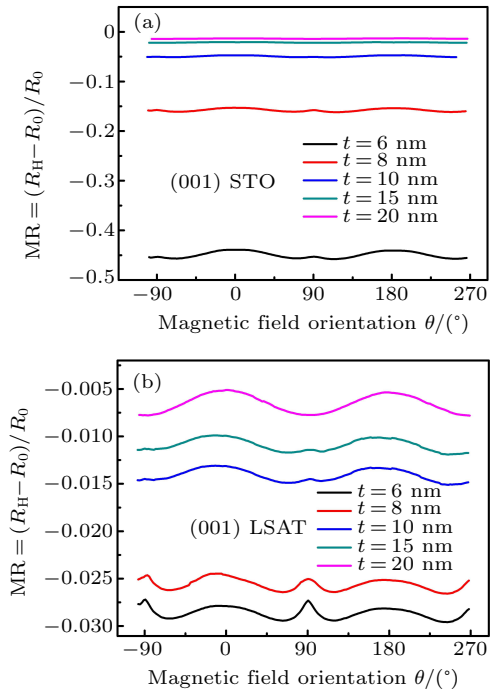


Fig. 7. Angular MR curves for LSMO films grown on (a) (001) STO substrate and (b) (001) LSAT substrate at 2 K and 8 T, respectively.

To investigate whether film orientation can influence the formation of 2DEG, the angular MR is measured for the LSMO films grown on STO and LSAT substrates with two different orientations at various temperatures. Figure 8 shows the angular MR curves of 6-nm-thick LSMO film. For the LSMO film grown on (001) STO [Fig. 8(a)], the LSMO/STO film at 2 K exhibits obvious four-fold symmetric MR, where four maxima appear at 0°, 180°, 90° and −90°. The pMR-peak is suppressed by increasing temperature. However, the peaks at 0° and 180° are enhanced with temperature increasing. For the film grown on (001) LSAT substrate [Fig. 8(c)], the evolution of angular MR curve is similar to that of the LSMO film grown on (001) STO substrate, which indicates that the strain state of film has no influence on the appearance of MR-peak. For the LSMO films grown on (001) LAO substrate [Fig. S7], no pMR-peak is observed even at a very low temperature of 2 K, indicating that the disappearance of the 2DEG is related with the existence of linear defects (as shown in Fig. 4) in the LSMO film grown on LAO substrate.

For the LSMO films grown on (011) STO [Fig. 8(b)] and (011) LSAT [Fig. 8(d)], only two pMR-peaks are found to appear at ±90°, which gradually disappear with temperature increasing. Comparing with the MR curves obtained from the LSMO films grown on (001) STO and (001) LSAT, the MR peaks at 0° and 180° disappear, which might be caused by magnetic anisotropy. The pMR-peaks at ±90° signal the formation of a two dimensional manganite at the film interface, which could arise from a magnetic reconstruction. With temperature increasing, the thermal motion of electron is intensified, which destroys the magnetic reconstruction. Therefore, the 2DEG is suppressed, and the pMR-peaks disappear gradually. From the above analysis, it can be concluded that film orientation has no influence on the formation of 2DEG.

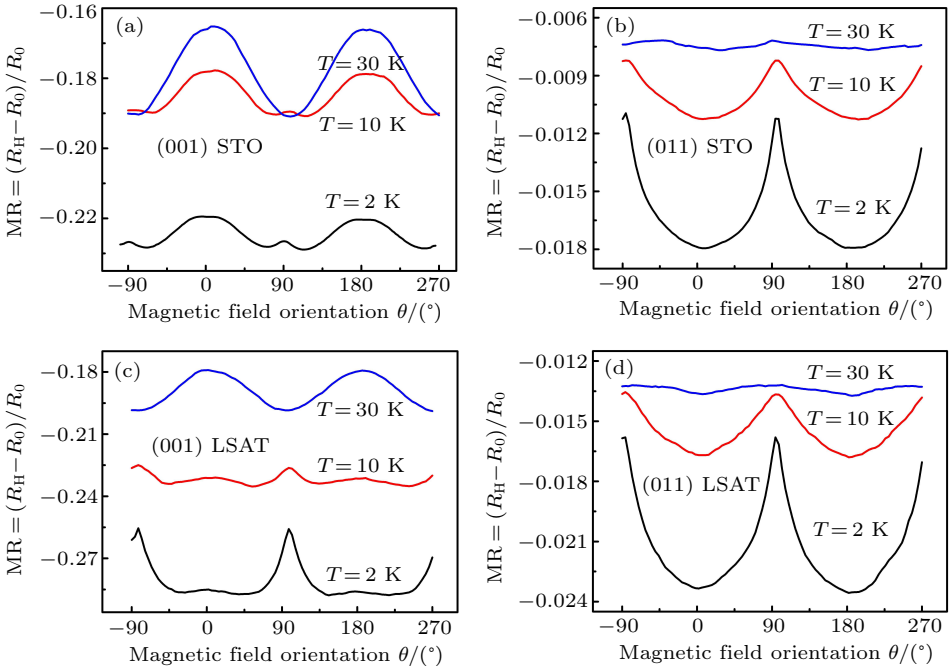


Fig. 8. Angular MR curves for LSMO films grown on (a) (001) STO, (b) (011) STO, (c) (001) LSAT, and (d) (011) LSAT, respectively.

To demonstrate the existence of magnetic anisotropy in LSMO films grown, respectively, on STO and LSAT substrates with two different orientations, magnetic hysteresis loops are measured. From Fig. 9, it can follow that the saturation moment of LSMO film grown on (011) STO (4.75×10^{-5} emu) substrate is larger than that grown on (001) STO (4.27×10^{-5} emu) substrate, and so are the saturation moments of LSMO films grown on (011) LSAT (4.78×10^{-5} emu) and (001) LSAT (4.25×10^{-5} emu) substrates. Thus, it is deduced that the difference in orientation of substrate has effect on the saturation moment of LSMO film. Additionally, because the hysteresis loss is proportional to the area that is surrounded by a magnetic hysteresis loop, it can be calculated that the hysteresis losses of LSMO films grown on (011) STO (1.09×10^{-5} J) and (011) LSAT (4.30×10^{-6} J) substrates are smaller than those grown on (001) STO (2.31×10^{-5} J) and (001) LSAT (1.10×10^{-5} J) substrates, respectively, which means lattice orientations of substrates can influence the hysteresis losses of films under the same measuring condition. The above-mentioned results might suggest the existence of magnetic anisotropy in LSMO films grown on STO and LSAT substrates with different orientations.

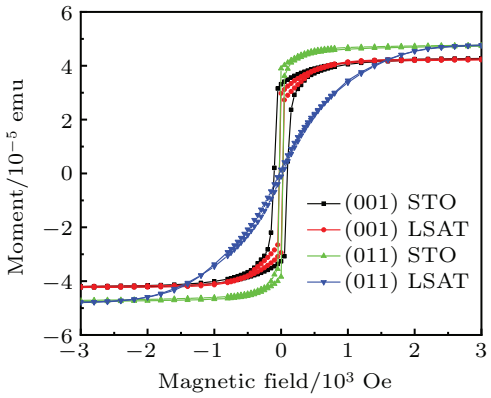


Fig. 9. Magnetic hysteresis loops of LSMO films with different substrate orientations at 10 K. The unit 1 Oe = 79.5775 A·m^{-1}.

4. Conclusions

In this work, in the LSMO films with small lattice mismatch, a resistivity upturn arises at low temperature when the film thickness is less than 15 nm, which is caused by WL effect. While the LSMO films with big lattice mismatch show a semiconductor behavior due to the linear defects. Besides, a sharp pMR peak emerges at low temperatures as the magnetic field rotates around the interface in LSMO film with small lattice mismatch, which is caused by 2DEG. The pMR peak disappears gradually with film thickness and temperature increasing. The film orientation has no influence on the formation of 2DEG.

References

[1] Wang L M and Guo C C 2005 *Appl. Phys. Lett.* **87** 172503
[2] Dey P, Nath T K and Taraphder A 2007 *Appl. Phys. Lett.* **91** 012511
[3] Malisa A and Ivanov Z 2005 *J. Magn. Magn. Mater.* **295** 277
[4] Lee H S, Choi S G, Park H H and Rozenberg M J 2013 *Sci. Rep.* **3** 1704
[5] Sharma H, Tulapurkar A and Tomy C V 2014 *Appl. Phys. Lett.* **105** 222406
[6] Ling Z B, Liu G J, Yang C P, Liang W S and Wang Y Q 2019 *Chin. Phys. B* **28** 046101
[7] Zener C 1951 *Phys. Rev.* **82** 403
[8] Takamura Y, Chopdekar R V, Arenholz E and Suzuki Y 2008 *Appl. Phys. Lett.* **92** 162504
[9] Cui B, Song C, Gehring G A, Li F, Wang G, Chen C and Pan F 2015 *Adv. Funct. Mater.* **25** 864
[10] Tsui F, Smoak M C, Nath T K and Eom C B 2000 *Appl. Phys. Lett.* **76** 2421
[11] Sirena M, Steren L and Guimpel J 2000 *Thin Solid Films* **373** 102
[12] Yang S Y, Kuang W L, Liou Y, Tse W S, Lee S F and Yao Y D 2004 *J. Magn. Magn. Mater.* **268** 326
[13] Maritato L, Adamo C, Barone C, De Luca G M, Galdi A, Orgiani P and Petrov A Y 2006 *Phys. Rev. B* **73** 094456
[14] Kondo J 1964 *Prog. Theor. Phys.* **32** 37
[15] Rozenberg E, Auslender M, Felner I and Gorodetsky G 2000 *J. Appl. Phys.* **88** 2578
[16] Niu W, Gao M, Wang X F, Song F Q, Du J, Wang X R, Xu Y B and Zhang R 2016 *Sci. Rep.* **6** 26081
[17] Zhang Y, Gan Y L, Niu W, Norrman K, Yan X, Christensen D V, von Soosten M, Zhang H R, Shen B G, Pryds N, Sun J R and Chen Y Z 2018 *ACS Appl. Mater. Inter.* **10** 1434
[18] Lee P A and Ramakrishnan T V 1985 *Rev. Mod. Phys.* **57** 287
[19] Lee P A and Ramakrishnan T V 1985 *Rev. Mod. Phys.* **57** 287
[20] Liu B, Wang Y Q, Liu G J, Feng H L, Yang H W and Sun J R 2016 *J. Appl. Phys.* **120** 154103
[21] Bergmann G 1984 *Phys. Rep.* **107** 1
[22] Shalom M B, Tai C W, Lereah Y, Sachs M, Levy E, Rakhmilevitch D, Palevski A and Dagan Y 2009 *Phys. Rev. B* **80** 140403
[23] Li X T, Liu B, Wang Y Q, Xue X Y, Liu G J, Yang H W and Sun J R 2018 *J. Am. Ceram. Soc.* **101** 2339